Journal of Materials Chemistry A

Accepted Manuscript

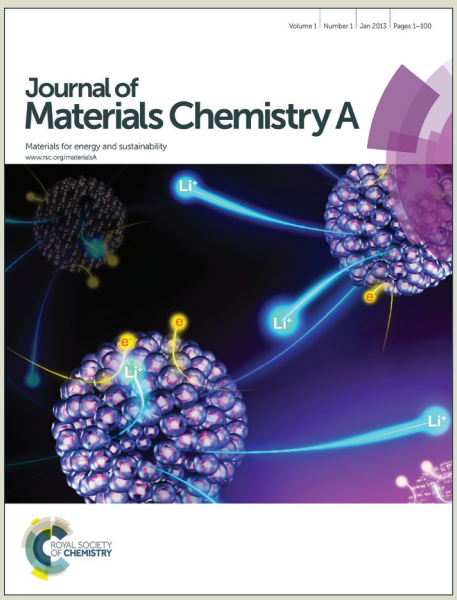

ROYAL SOCIETY OF CHEMISTRY

www.rsc.org/materialsA

Journal Name

ARTICLE

Size and Bandgap Tunability in Bi_2S_3 Colloidal Nanocrystals and its Effect in Solution Processed Solar Cells

María Bernechea,*[a] Yiming Cao,[a] and Gerasimos Konstantatos*[a]

Received 00th January 20xx,
Accepted 00th January 20xx

DOI: 10.1039/x0xx00000x

www.rsc.org/

We report the synthesis and full characterization of colloidal Bi_2S_3 nanocrystals with different sizes, showing a band gap variation up to 0.2 eV, and pointing to quantum confinement effects. Polymer-nanocrystal solar cells have been fabricated to study the effect of the size, and band gap change, on the performance of the devices. We have found that smaller nanocrystals present a much higher Voc, pointing to a system with reduced density of surface traps.

Introduction

Bismuth sulfide (Bi_2S_3) is a semiconductor with a wide range of applications such as electrochemical hydrogen storage, X-ray computed tomography, thermoelectrics, or photocatalysis.[1–6] Moreover, due to its favorable band gap and high absorption coefficient, it has been used in optoelectronic applications such as photodetectors or solar cells.[7–9] In addition, it presents an n-type character and it is composed of earth-abundant non-toxic elements, which allows for the fabrication of solar cells based on low toxicity materials when combined with conductive polymers.[10–14] The reported band gap values for polycrystalline samples vary between 1.3 eV and 1.7 eV, without conclusive evidence on the origins of this deviation, typically attributed to stoichiometric variability or quantum confinement effects. However, there are very few cases in which the quantum confinement effects have been studied, synthesizing particles with different sizes and measuring the corresponding band gaps.[15–19] The largest tunability range in the bandgap of Bi_2S_3 nanocrystals has been ≈0.10 eV, but the size of the nanocrystals was not directly measured by TEM,[17] or the band gap was not clearly determined.[15] In a more recent study, nanocrystals with sizes between 3 and 30 nm were synthesized and the band gap variation was found to be as small as 0.03 eV.[18] Recent theoretical calculations suggest that quantum confinement effects should be weak for nanocrystals larger than 3 nm and variations larger than 0.1 eV are not to be expected, while changes up to 0.5 – 0.8 eV could reached for nanoparticles smaller than 3 nm.[18,20] Therefore, the effect of employing Bi_2S_3 nanocrystals with different sizes and/or band gaps, thus in the form of colloidal quantum dots, in solar cells has not been reported yet.

In order to verify the afore-mentioned reports and to further explore the potential of this semiconductor as a quantum confined material, we have synthesized Bi_2S_3 nanocrystals (NCs) with three different sizes: spherical particles with 2.6 and 4.1 nm diameters, and nanorods with 14x19 nm dimensions. The changes in size are followed by changes in band gap up to 0.2 eV among them, and 0.3 eV with respect to the band gap of the material in bulk (1.3 eV). Moreover, we have measured the associated modifications of the conduction and valence band energy positions, and we have fabricated polymer-NC solar cells, finding relevant effects in the efficiency of the devices.

Experimental Section

Chemicals and Materials.

All the reactions were carried out using standard Schlenk techniques. Reagents were purchased from Sigma Aldrich, except $Bi(OAc)_3$ which was purchased from Alfa Aesar and Poly(3-hexylthiophene) (P3HT) which was purchased from Rieke Metals.

Synthesis of Bi_2S_3 nanocrystals.

Synthesis of Bi_2S_3 nanorods (14 x 19 nm). The synthesis of Bi_2S_3 nanocrystals was performed using a modification of the previously reported procedure.[21] Briefly, 2.8 mmol of $Bi(OAc)_3$ and 34 mmol of oleic acid (OA) were pumped overnight at 100ºC. After this time, the reaction temperature was raised to 170ºC. When the reaction flask reached this temperature 0.6 mmol of HMS (Hexamethyldisilathiane) mixed with 5 ml of 1-Octadecene (ODE) were quickly injected to the flask and the heating temperature was lowered to 100ºC. After 2 h at 100ºC the reaction was quenched by removing the heating mantle and adding 10 ml of cold toluene and 20 ml of cold methanol. The oleate caped Bi_2S_3 nanocrystals were isolated after centrifugation. Purification of the nanocrystals was performed by successive dispersion/precipitation in toluene/MeOH. Finally the nanocrystals were dispersed in anhydrous toluene.

Synthesis of small Bi_2S_3 (2.6 and 4.1 nm). 2.8 mmol of $Bi(OAc)_3$ and 34 mmol of OA were pumped overnight at 100ºC. After this

[a] ICFO – Institut de Ciències Fotòniques, Mediterranean Technology Park, Av. Carl Friedrich Gauss, 3. 08860. Castelldefels (Barcelona), Spain. E-mail: maria.bernechea@icfo.es; gerasimos.konstantatos@icfo.es

† Electronic Supplementary Information (ESI) available. See DOI: 10.1039/x0xx00000x

time, the reaction temperature was reduced to 50ºC. When the reaction flask reaches this temperature 0.6 mmol of HMS mixed with 5 ml of ODE were quickly injected to the flask. For the 2.6 nm NCs, when the colour of the reaction changed to orange (10 – 20 sec), the flask was quickly immersed in an ice bath. For the 4.1 nm NCs, the NCs were allowed to grow at 50ºC for 4 h and after that time the flask was immersed in an ice bath. Once the flasks were in the ice bath, 10 ml of cold toluene and 40 ml of cold acetone were injected to quench the reaction. The oleate caped Bi_2S_3 nanocrystals were isolated after centrifugation and further purified by successive dispersion/precipitation in toluene/acetone. Finally the nanocrystals were dispersed in anhydrous toluene.

Characterization of Bi_2S_3 nanocrystals.

Absorption measurements were performed using a Cary 5000 UV-VIS-NIR spectrophotometer, in solution on a glass cuvette of 1 mm optical path or as films on glass substrates.

Confocal Raman microspectroscopy was performed in a Renishaw system using a 785-nm laser at 0.05 % laser power. Samples were prepared by covering a glass substrate with the toluene solutions and allowing the solvent to evaporate in air.

TEM and XRD measurements were performed in the Scientific and Technological Centres of the University of Barcelona (CCiT-UB).

Transmission electron microscopy (TEM) micrographs were obtained using a JEOL 2100 microscope, operating at an accelerating voltage of 200 kV. The microscope is equipped with an INCA detector for EDX (Energy-dispersive X-ray spectroscopy) analysis (detection limit of 1 – 0.1 at% and a standard deviation of 10%). Samples were prepared by placing two drops of a diluted toluene solution on a holey-carbon-coated grid and allowing the solvent to evaporate in air. The average diameter was calculated by measuring the diameters of no less than 100 nanocrystals from non-aggregated areas.

X-Ray Diffraction (XRD) data were collected using a PANalytical X'Pert PRO MPD Alpha1 powder diffractometer in Bragg-Brentano θ/2θ geometry of 240 millimeters of radius, Cu Kα radiation: λ = 1.5406 Å and work power: 45 kV – 40 mA. Samples were prepared by covering a glass (approximately of 20 mm x 20 mm) with the toluene solutions of nanocrystals and allowing it to evaporate in air.

UV photoelectron spectroscopy (UPS) and X-ray photoelectron spectroscopy (XPS) measurements were performed in Institut Català de Nanociencia Nanotecnologia i (ICN2).

XPS and UPS measurements were performed on a SPECS PHOIBOS 150 electron spectrometer analyser (SPECS GmbH, Berlin, Germany) in ultra-high vacuum conditions (base pressure 1E-10 mbar), using the monochromatic HeI radiation (21.2 eV) for UPS and a monochromatic K-alpha X-Ray source (1486.74 eV) for XPS. The pass energy values used was 10 eV for the high resolution spectrum and the energy resolution as measured by the FWHM of the Ag $3d_{5/2}$ peak for a sputtered silver foil was 0.55 eV (detection limit 1 – 0.1 at%). Intensities were estimated by calculating the integral of each peak, determined by subtracting the Shirley-type background and fitting the experimental curve to a combination of Lorentzian and Gaussian lines of variable proportions. The atomic amount of each element was calculated using the Wagner atomic sensitivity factors (10% standard deviation).[22] Accurate binding energies (0.2eV) were determined by referencing to the C 1s peak at 284.8 eV. Samples were prepared by covering ITO substrates (approximately 10 x 10 mm) with the toluene solutions and allowing the solvent to evaporate in air.

Fast Fourier Infrared spectroscopy (FTIR) measurements were performed on a Cary 600 FTIR spectrophotometer in transmission mode. Samples were placed on KBr substrates.

Device Fabrication.

ITO substrates were cleaned thoroughly by water, acetone and 2-propanol and dried using a nitrogen gun prior to device preparation. A ZnO electron transport layer was grown using a sol–gel method. Briefly, 0.5 g of zinc acetate dihydrate was dissolved in 5 mL of methoxyethanol and 0.142 mL of ethanolamine. The solution was spin-cast onto the ITO-coated glass substrates at 3000 rpm and annealed at 200ºC for 30 minutes. This process is done twice. Solutions of 20 g/l of Bi_2S_3 NCs were prepared adding toluene to the original highly concentrated solution. The desired film thickness was obtained via layer-by-layer spin coating process. One drop of NCs was dispensed on top of a spinning (2000 rpm) substrate, followed by 3 drops of 1,2-ethanedithiol (EDT) 2% vol. in acetonitrile. The ligand was left reacting for 20 seconds prior to the dispensing of a flush of acetonitrile and a flush of toluene. A 50 mg/ml P3HT solution in dichlorobenzene was prepared by stirring overnight at 50ºC. A P3HT layer was spincoated onto the Bi_2S_3 films at 3000 rpm spin velocity for 2 minutes. Before metal deposition the films were annealed for 15 minutes at 100ºC. Metal deposition was carried out on Kurt J. Lesker Nano 36 system at a base pressure lower than $5x10^{-6}$ mbar. Final thickness was controlled together with deposition rate monitoring via a quartz crystal. A thin layer of molybdenum oxide (5 nm, 0.1 $Å s^{-1}$ deposition rate) followed by 150 nm of Ag (2 $Å s^{-1}$) were deposited to achieve the top electrical contact. Device area was determined by a shadow circular mask of 2mm in diameter.

Device Characterization.

All device characterization was performed in ambient conditions. Current-voltage characteristics were obtained using a Keithley 2400 source measuring unit under dark and simulated AM1.5G 100 mW/cm^2 illumination conditions (Newport 96000). External quantum efficiency (EQE) measurements were obtained using a Newport Cornerstone 260 monochromator and a Keithley 2400 source measuring unit providing shortcircuit conditions.

Results and discussion

We have previously reported the synthesis of 14x19 nm Bi_2S_3 nanorods with ≈1.3 eV band gap (Fig. 1a).[21] By reducing the injection temperature of HMS (Hexamethyldisilathiane) to 50 ºC, the size of the nanocrystals can be reduced to 2.6 nm (Fig. 1c). Upon further growth at 50 ºC for 4 hours, the size increases to 4.1 nm (Fig. 1b).

When the nanocrystals are allowed to grow for one hour, the size is 3.8 nm, similar to the NCs grown for 4 hours, but the size dispersion is higher (Fig. S1, Supporting Information).

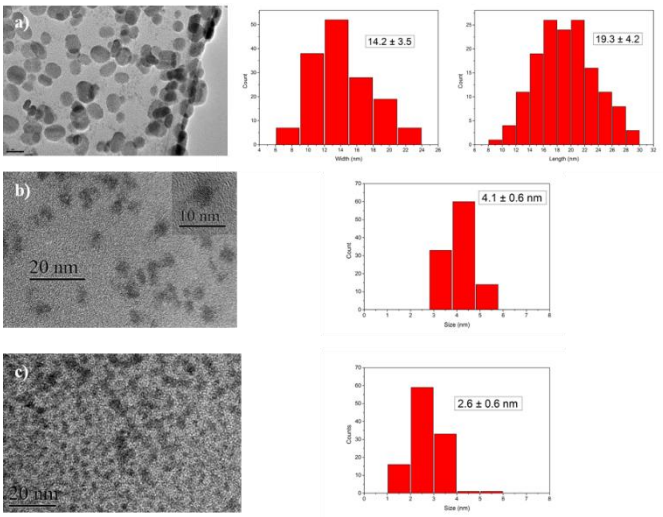

Fig 1 a) TEM micrograph of 14x19 nm Bi_2S_3 nanorods and the corresponding size distribution of length and width. Scale bar is 20 nm. b) TEM micrograph of Bi_2S_3 nanocrystals with 4.1 nm diameter (left), and size distribution calculation (right). Inset shows a micrograph with higher magnification. c) TEM micrograph and size distribution of 2.6 nm nanocrystals.

The TEM micrographs also reveal the crystallinity of the samples. The inset in Fig. 1b shows a higher magnification micrograph where the planes of the nanocrystal are visible. The Fast Fourier Transform of this image gives d-spacing values of 0.32 and 0.22 nm, which correspond to the (230) and (421) interplanar distances of orthorhombic Bi_2S_3 (ref. 00-006-0333). The XRD pattern of the 14x19 nm nanorods fits with the reference (Fig. 2a), while for the smaller nanocrystals lines encompassing several peaks are observed. The relative intensity of the peaks changes for the smaller NCs, consistent with the different shape. The Raman spectra further support the crystallinity of the samples (Fig. 2b), showing peaks at 167, 183, 235 and 259 cm^{-1}, consistent with previously reported data.[14,23–25] It is obvious that larger nanocrystals exhibit more defined peaks in XRD or Raman spectra, as expected for samples with larger crystalline domains.

The changes in size have a direct impact in the band gap that

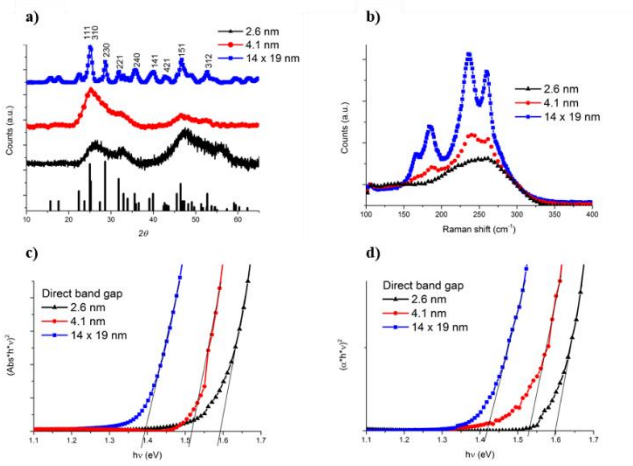

Fig. 2 a) XRD patterns and reference pattern for orthorhombic Bi_2S_3, Ref.: 00-006-0333. b) Raman spectra. c) Tauc plot of nanocrystals with different sizes in toluene solution. d) Tauc plot of films prepared with EDT treated nanocrystals of different sizes.

Table 1 Relative atomic amounts found by XPS[a)]

Sample	C	O	S (2s)	Bi/S	Formula
2.6 nm	12.9	3.3	0.66	1.52	$Bi_2S_{1.3}$
2.6 nm-EDT	1.8	0.3	1.66	0.60	$Bi_2S_{3.3}$
4.1 nm-EDT	1.5	0.2	1.58	0.63	$Bi_2S_{3.2}$
14x19 nm-EDT	1.3	0.4	1.46	0.68	$Bi_2S_{2.9}$

a) Quantities normalized to bismuth

increases from 1.39 eV (≈1.4 eV), corresponding to the 14x19 nm nanorods, to 1.52 (≈1.5 eV) and 1.59 eV (≈1.6 eV), for nanocrystals with sizes 4.1 and 2.6 nm, respectively (Fig. 2c).

It could be claimed that the difference in band gap arises from differences in stoichiometry.[26] Indeed, EDX analyses performed during TEM measurements confirm an excess of bismuth in all the samples, which is even higher in the smaller crystals (Bi/S ratio: 1.54 for 2.6 nm NCs; 1.25 for 4.6 nm NCs and 0.97 for 14x19 nm nanorods). However, measurements of the band gap in film, after treatment with ethanedithiol ligands (EDT), which gives nearly stoichiometric ratios of 0.67 (see elemental ratios extracted from XPS analysis in Table 1), preserve the same trend (Fig. 2d). This points to the fact that changes in band gap are due to changes in size, thereby indicating the appearance of quantum size effects, reported for the first time for this semiconductor compound. Apart from the bismuth to sulfur ratio, Table 1 shows that the EDT treatment is effective in removing the original oleic acid capping ligands and prevents oxidation of the samples. The substitution of oleic acid by EDT has been additionally confirmed by FTIR (Fig S2).

For all the samples analyzed, the Bi 4f core-level spectrum analyzed by XPS can be deconvoluted into two contributions (Fig S3). The binding energy position and relative abundance of these peaks are summarized in Table 2. For the bare sample, without EDT treatment, the peak appearing at 158.5 can be attributed to Bi-S bonds, while the one appearing at 159.1 can be ascribed to Bi-S species with some degree of oxidation.[16] The latter refers to bismuth atoms located on the surface of the nanocrystals, where they are bonded to sulfur and to oxygen atoms, either this being from the oleic acid ligands or due to some oxidation of the surface.

For the EDT treated samples this peak at high binding energies disappears, but again two contributions are detected, one at 158 eV and a second one at 158.2 eV. Both appear at higher binding energies than those corresponding to elemental bismuth (≈162 and ≈157 eV),[16,27,28] and can be attributed to Bi-S bonds. However, it is remarkable that they appear at quite low binding energies, especially the one at 158 eV, and indicate a high concentration of electron density on the bismuth atoms, which is higher in the 14x19 nanorods than in the smaller nanocrystals (66 % *vs.* 32 and 20 %). In small nanoparticles most of the atoms are located on the surface, while in larger nanocrystals is the contrary. The fact that this lower energy contribution is higher in the nanorods indicates that this concentration of electron density is mostly supported by

Table 2 Binding Energies (eV) and Surface Atomic Ratios of Samples[a)]

Sample	Bi $4f_{7/2}$	Bi $4f_{5/2}$
2.6 nm	158.5 (57)	163.9
	159.1 (43)	164.5
2.6 nm-EDT	158.1 (32)	163.7
	158.2 (68)	163.5
4.1 nm-EDT	158.0 (20)	163.7
	158.1 (80)	163.4
14x19 nm-EDT	158.1 (66)	163.4
	158.2 (34)	163.7

a) Binding energies (eV) are referred to the C 1s peak at 284.8 eV.

bismuth atoms located in the inside of the nanocrystals. This may be favored by the crystal structure of orthorhombic bismuth sulfide. This structure is composed of tightly connected chains creating layers that stack to form the final structure.[3,18,20,25,29] The layers are connected through weak Van der Waals forces, involving the unbounded electron lone pair of the bismuth atoms, which generates an electron cloud where "extra" electron density could easily be located. Additionally, the contribution at 158 eV is indicative of the n-type character of Bi_2S_3 films. Several studies have reported that the bottom of the conduction band comprises bismuth states.[25,29] An increase of electron density on bismuth atoms would then populate states close to the conduction band, indicating n-type doping. Indeed, this hypothesis is in agreement with the fact that the 14x19 nanorod film, presenting the higher 158 eV relative ratio, is the sample with the Fermi level closer to the conduction band (Fig. 3a).

The position of the Fermi level and the valence band of the samples has been determined by UPS measurements, while the position of the conduction band has been calculated taking into account the value of the band gap (Fig. S4). It should be noted that these measurements can only be performed in EDT treated nanocrystals and not in nanocrystals capped with oleic acid, because these long chain ligands are too insulating to obtain meaningful values by UPS.[30]

The data obtained for the 14x19 nm nanorods are in line with previous measurements,[8,9,21] and show that these films are heavily doped, with the Fermi level close to the conduction

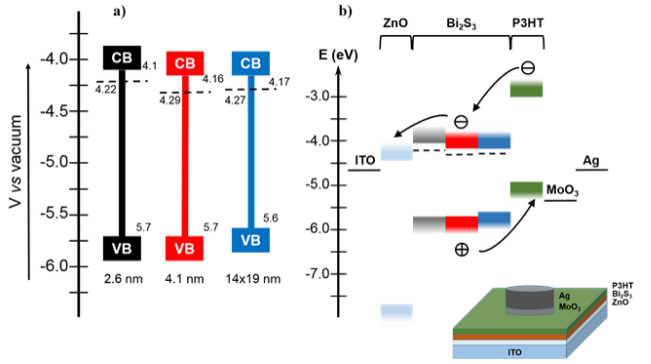

Fig 3 a) Energy level diagrams of the Bi_2S_3 nanocrystals with different sizes extracted form UPS measurements. b) Band diagram and charge transfer mechanism between the components of the solar cells fabricated for this study and schematic representation of the device architecture.

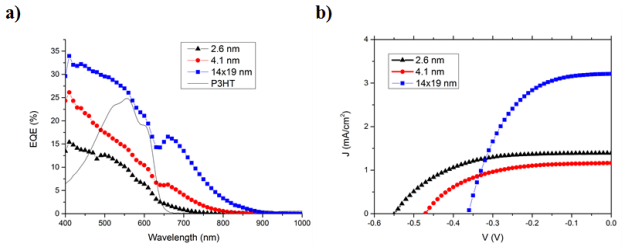

Fig. 4 a) External Quantum Efficiency (EQE) of the devices overlapped with the absorption of P3HT. b) J-V characteristics of the solar cells fabricated with Bi_2S_3 nanocrystals of different sizes.

band (Fig. 3a). All the films are clearly n-type, and the main variation with size is the decrease in energy of the conduction band, while the valence band and the Fermi level remain nearly unchanged with a maximum variation of 0.07 V. To test the effect that the different properties of the synthesized nanocrystals have in the performance of solar cells, we fabricated devices whose architecture is depicted in Fig. 3b. In brief, they consist of a sol-gel zinc oxide layer grown on ITO coated glass, that has the double function of acting as electron transport layer (ETL) and as hole blocking layer (Fig. 3b). On top of the ZnO layer the Bi_2S_3 layer has been deposited, followed by a P3HT hole transport layer (HTL), an evaporated molybdenum oxide (MoO_3) and silver (Ag) electrode. The Bi_2S_3 layer was fabricated by employing a layer-by-layer (LBL) technique by repeated spin coating of nanocrystals followed by EDT treatment as the crosslinking molecule (see experimental section). The thicknesses of the Bi_2S_3 and P3HT layers are ≈60 and ≈120 nm respectively, for comparison with previously reported data.[10,12,13] The EQE spectra and current-voltage curves are depicted in Fig. 4a and Fig. 4b, respectively, and the obtained values for champion devices are summarized in Table 3.

The highest EQE and the best efficiency correspond to the device fabricated employing the bigger 14x19 nm nanorods, however it should be noted that the fabrication process and thickness of the layers have been previously optimized for this kind of nanocrystals.[10,12] Interestingly, the devices fabricated with the smaller nanocrystals present a decent performance, mainly due to an increase in Voc by nearly 0.2 V, from 0.36 V of the large NCs to 0.47 and 0.55 V for 4.1 and 2.6 nm, respectively. Although these devices suffer from low currents, the values are comparable to recently reported devices with similar thickness,[13] and overall efficiency could be further improved

Table 3 Solar cell performance parameters of champion devices in this study Open circuit voltage (Voc), short circuit current density (Jsc), predicted current extracted from EQE (EQE Jsc), fill factor (FF), power conversion efficiency (PCE) series resistance (Rs) and shunt resuistance (Rsh).

Sample	V_{OC} [V]	J_{SC} [mA/cm²]	EQE J_{SC} [mA/cm²]	FF	PCE [%]	Rs (kΩ)	Rsh (kΩ)
2.6 nm	0.55	1.39	1.68	0.56	0.43	1.44	0.657
4.1 nm	0.47	1.16	2.64	0.53	0.29	0.604	0.223
14x19 nm	0.36	3.21	5.13	0.52	0.60	0.447	0.140

by optimizing the device architecture, varying the active layer thickness or using a bulk heterojunction.[11–13] It should be noted that this variation in V_{OC} with nanocrystal size has been found in several devices (see Table S1).

It is interesting to note that the increase in Voc for the smaller nanocrystals (0.2 V) is not related to changes in the position of the Fermi level (0.07 V variation between samples, Fig. 3a). Since it has been previously reported that surface traps limit the Voc of this system,[10,12] the origin of the Voc increase lies upon a better trap passivation in the smaller NCs. Moreover, the higher shunt resistance, and better agreement between the measured current and predicted EQE current found for the smaller NCs (83% agreement for champion device, table 3, and 67% agreement for average value, table S1), also points to a system with suppressed trap-assisted recombination, as compared to the larger NCs (43% and 62% for 4.1 and 14x19 nm NCs champion devices, respectively). The origin of this improved trap passivation can be geometrical, either because spherical shapes generate less steric hindrance for the surface ligands than the nanorods, or, depending on the size, different facets stay on the surface and present different reactivity towards the EDT ligands added to replace the oleic acid ligands and passivate the surface defects.[31,32] Indeed, taking into account the Bi/S ratio extracted from EDX and XPS measurements, before and after EDT treatment, it is clear that the smaller nanocrystals are able to allocate more EDT ligands on the surface than the nanorods, allowing thus for a better surface passivation.

Conclusions

In summary, we have synthesized and fully characterized Bi_2S_3 nanocrystals with different sizes, from nanoparticles of 2.6 nm to nanorods with 14x19 nm dimensions. We have demonstrated that the band gap of Bi_2S_3 can be tuned up to 0.2 eV and that this change is due to quantum confinement effects. The change in band gap is accompanied by a change in the band level positions, while the Fermi level remains nearly unchanged. However, the devices fabricated with the smaller nanocrystals present a much higher Voc pointing to a system with reduced density of surface traps and paving the way for further exploration of Bi_2S_3 as a potential photoactive material in photovoltaics.

Acknowledgements

We acknowledge Fundació Privada Cellex, European Commission's Seventh Framework Programme for Research under contract PIRG06-GA-2009-256355 and European Community's Seventh Framework program (FP7-ENERGY.2012.10.2.1) under grant agreement 308997 for financial support.

Notes and references

1 O. Rabin, J. Manuel Perez, J. Grimm, G. Wojtkiewicz and R. Weissleder, *Nat. Mater.*, 2006, **5**, 118–22.
2 L. Li, N. Sun, Y. Huang, Y. Qin, N. Zhao, J. Gao, M. Li, H. Zhou and L. Qi, *Adv. Funct. Mater.*, 2008, **18**, 1194–1201.
3 K. Biswas, L.-D. Zhao and M. G. Kanatzidis, *Adv. Energy Mater.*, 2012, **2**, 634–638.
4 J. Liu, X. Zheng, L. Yan, L. Zhou, G. Tian, W. Yin, L. Wang, Y. Liu, Z. Hu, Z. Gu, C. Chen and Y. Zhao, *ACS Nano*, 2015, **9**, 696–707.
5 J. Zhou, G. Tian, Y. Chen, Y. Shi, C. Tian, K. Pan and H. Fu, *Sci. Rep.*, 2014, **4**, 4027.
6 X. Gao, H. Bin Wu, L. Zheng, Y. Zhong, Y. Hu and X. W. D. Lou, *Angew. Chemie*, 2014, **126**, 6027–6031.
7 G. Konstantatos, L. Levina, J. Tang and E. H. Sargent, *Nano Lett.*, 2008, **8**, 4002–4006.
8 A. K. Rath, M. Bernechea, L. Martinez and G. Konstantatos, *Adv. Mater.*, 2011, **23**, 3712–3717.
9 A. K. Rath, M. Bernechea, L. Martinez, F. P. G. De Arquer, J. Osmond and G. Konstantatos, *Nat. Photonics*, 2012, **6**, 529 – 534.
10 L. Martinez, M. Bernechea, F. P. G. de Arquer and G. Konstantatos, *Adv. Energy Mater.*, 2011, **1**, 1029–1035.
11 L. Martinez, S. Higuchi, A. J. MacLachlan, A. Stavrinadis, N. C. Miller, S. L. Diedenhofen, M. Bernechea, S. Sweetnam, J. Nelson, S. a. Haque, K. Tajima and G. Konstantatos, *Nanoscale*, 2014, **6**, 10018.
12 L. Martinez, A. Stavrinadis, S. Higuchi, S. L. Diedenhofen, M. Bernechea, K. Tajima and G. Konstantatos, *Phys. Chem. Chem. Phys.*, 2013, **15**, 5482–5487.
13 L. Whittaker-Brooks, J. Gao, A. K. Hailey, C. R. Thomas, N. Yao and Y.-L. Loo, *J. Mater. Chem. C*, 2015, **3**, 2686–2692.
14 A. J. Maclachlan, F. T. F. O'Mahony, A. L. Sudlow, M. S. Hill, K. C. Molloy, J. Nelson and S. a. Haque, *ChemPhysChem*, 2014, **15**, 1019–1023.
15 D. J. Riley, J. P. Waggett and K. G. U. Wijayantha, *J. Mater. Chem.*, 2004, **14**, 704.
16 R. Malakooti, L. Cademartiri, Y. Akçakir, S. Petrov, a. Migliori and G. a. Ozin, *Adv. Mater.*, 2006, **18**, 2189–2194.
17 B. Pejova and I. Grozdanov, *Mater. Chem. Phys.*, 2006, **99**, 39–49.
18 M. Aresti, M. Saba, R. Piras, D. Marongiu, G. Mula, F. Quochi, A. Mura, C. Cannas, M. Mureddu, A. Ardu, G. Ennas, V. Calzia, A. Mattoni, A. Musinu and G. Bongiovanni, *Adv. Funct. Mater.*, 2014, **24**, 3341–3350.
19 P. Han, A. Mihi, J. Ferre-borrull, J. Pallarés and L. F. Marsal, *J. Phys. Chem. C*, 2015, **119**, 10693–10699.
20 V. Calzia, G. Malloci, G. Bongiovanni and a. Mattoni, *J. Phys. Chem. C*, 2013, **117**, 21923–21929.
21 Y. Cao, M. Bernechea, A. Maclachlan, V. Zardetto, M. Creatore, S. a. Haque and G. Konstantatos, *Chem. Mater.*, 2015, **27**, 3700−3706.
22 C. D. Wagner, L. E. Davis, M. V Zeller, J. a Taylor, R. H. Raymond and L. H. Gale, *Surf. Interface Anal.*, 1981, **3**, 211–225.
23 K. Trentelman, *J. Raman Spectrosc.*, 2009, **40**, 585–589.
24 F. Lu, R. Li, Y. Li, N. Huo, J. Yang, Y. Li, B. Li, S. Yang, Z. Wei and J. Li, *ChemPhysChem*, 2015, **16**, 99–103.
25 Y. Zhao, K. T. E. Chua, C. K. Gan, J. Zhang, B. Peng, Z. Peng and Q. Xiong, *Phys. Rev. B - Condens. Matter Mater. Phys.*, 2011, **84**, 205330–1–8.
26 P. S. Sonawane and L. a. Patil, *Mater. Chem. Phys.*, 2007, **105**, 157–161.
27 S. ten Haaf, B. Balke, C. Felser and G. Jakob, *J. Appl. Phys.*, 2012, **112**, 053705.
28 J. Grigas, E. Talik and V. Lazauskas, *Phys. status solidi*, 2002, **232**, 220–230.
29 M. R. Filip, C. E. Patrick and F. Giustino, *Phys. Rev. B - Condens. Matter Mater. Phys.*, 2013, **87**, 205125–1/205125–11.
30 P. R. Brown, D. Kim, R. R. Lunt, N. Zhao, M. G. Bawendi, J. C. Grossman and V. Bulovi, *ACSNano*, 2014, **8**, 5863–5872.

31 J. Tang, L. Brzozowski, D. A. R. Barkhouse, X. Wang, R. Debnath, R. Wolowiec, E. Palmiano, L. Levina, A. G. Pattantyus-Abraham, D. Jamakosmanovic and E. H. Sargent, *ACS Nano*, 2010, **4**, 869–878.
32 H. Choi, J. Ko, Y. Kim and S. Jeong, *J. Am. Chem. Soc.*, 2013, **135**, 5278−5281.

Size and Bandgap Tunability in Bi_2S_3 Colloidal Nanocrystals and its Effect in Solution Processed Solar Cells

María Bernechea, Yiming Cao, and GerasimosKonstantatos

Band gap tunability with size is presented for colloidal Bi_2S_3nanocrystals and the effect in solar cells is studied.